

Reliability improvement of nonlinear ultrasonic modulation based fatigue crack detection using feature-level data fusion

Hyung Jin Lim, Yongtak Kim, Hoon Sohn*, Ikgeun Jeon and Peipei Liu

Department of Civil and Environmental Engineering, Korea Advanced Institute for Science and Technology,
291 Daehak-ro, Yuseong-gu, Daejeon 34141, Republic of Korea

(Received January 15, 2017, Revised November 11, 2017, Accepted December 1, 2017)

Abstract. In this study, the reliability of nonlinear ultrasonic modulation based fatigue crack detection is improved using a feature-level data fusion approach. When two ultrasonic inputs at two distinct frequencies are applied to a specimen with a fatigue crack, modulation components at the summation and difference of these two input frequencies appear. First, the spectral amplitudes of the modulation components and their spectral correlations are defined as individual features. Then, a 2D feature space is constructed by combining these two features, and the presence of a fatigue crack is identified in the feature space. The effectiveness of the proposed fatigue crack detection technique is experimentally validated through cyclic loading tests of aluminum plates, full-scale steel girders and a rotating shaft component. Subsequently, the improved reliability of the proposed technique is quantitatively investigated using receiver operating characteristic analysis. The uniqueness of this study lies in (1) improvement of nonlinear ultrasonic modulation based fatigue crack detection reliability using feature-level data fusion, (2) reference-free fatigue crack diagnosis without using the baseline data obtained from the intact condition of the structure, (3) application to full-scale steel girders and shaft component, and (4) quantitative investigation of the improved reliability using receiver operating characteristic analysis.

Keywords: fatigue crack; nonlinear ultrasonic modulation; structural health monitoring; data fusion; receiver operating characteristic analysis

1. Introduction

A fatigue crack, which is one of the primary culprits behind the failure of metallic structures, is initiated from a damage precursor at an unperceivable level (e.g., dislocation or micro crack in materials) when the material is subjected to repeated loading. The crack often continues to grow to a critical point and leads to unexpected failure without proper warning. It is estimated that up to 90% of failures of in-service metallic structures are the result of fatigue cracks (Campbell 2008). Additionally, a fatigue crack becomes conspicuous only after the crack reaches approximately 80% of the total fatigue life of the structure (Camarata *et al.* 2010, Kim *et al.* 2011). For example, in 1994, the middle span of Seongsu Bridge in Seoul, South Korea, suddenly fell into the Han River, and this incident resulted in 49 casualties. A later investigation discovered that fatigue failure of the welded joints due to repeated traffic loadings caused the collapse of the bridge (JST Failure Knowledge Database 2016).

Recently, nonlinear ultrasonic techniques have emerged as promising structural health monitoring (SHM) and nondestructive testing (NDT) techniques due to their higher sensitivity to early-stage micro fatigue cracks than conventional linear ultrasonic techniques (Jhang 2009,

Hong *et al.* 2014, Yim *et al.* 2016, Kim *et al.* 2016, Lim *et al.* 2016). Nonlinear ultrasonic techniques detect a fatigue crack by focusing on nonlinear components, such as harmonics and modulations created by a source of nonlinearity, e.g., a fatigue crack. When a single frequency ultrasonic wave propagates through a localized fatigue crack, additional components at harmonics of the input frequency occur (Cantrell and Yost 1994, Zhou *et al.* 2013). On the other hand, when two ultrasonic waves at two distinct frequencies are applied to a structure with a fatigue crack, the interaction of the input ultrasonic waves produces nonlinear modulation at the sum and difference of the two input frequencies (Croxford *et al.* 2009, Klepka *et al.* 2011).

A fatigue crack in a mild steel beam was detected using an impact hammer for low-frequency (LF) excitation and a surface-mounted lead zirconate titanate (PZT) transducer for high-frequency (HF) excitation (Duffour *et al.* 2006). Using a piezoelectric stack actuator for the generation of an LF input and a PZT transducer for an HF input, a fatigue crack in an aluminum plate was detected (Parsons and Staszewski 2006). Additionally, both LF and HF inputs were created by two PZT transducers, and bolt-loosening in aluminum plates and delamination in composites were detected (Amerini and Meo 2011, Chrysochoidis *et al.* 2011). Yoder and Adams (2010) used fixed LF and swept HF signals to find an optimal combination of LF and HF signals that could amplify the modulation due to a fatigue crack. A fatigue crack in an aircraft fitting-lug mock-up specimen was detected by sweeping both LF and HF input frequencies (Sohn *et al.* 2014). Automated fatigue crack

*Corresponding author, Professor
E-mail: sohnhoon@kaist.ac.kr

detection techniques without using the baseline data obtained from the intact condition of the structure have been developed and validated under various temperatures and loading conditions (Lim *et al.* 2014, 2016, Liu *et al.* 2016).

For field applications, damage diagnosis methods should be able to achieve high reliability by minimizing false alarms, and data fusion is considered one way of improving diagnostic reliability. Data fusion combines data from multiple sensors and information from associated databases to achieve improved accuracy and more specific inferences than could be achieved by the use of a single sensor (or information) alone (Hall and Llinas 1997). Indeed, data fusion is usually performed at three different levels: data-level, feature-level and decision-level. In data-level fusion, all measured data are combined first and further processed for decision making. In feature-level fusion, features are extracted from each sensor (or data), the extracted features are concatenated into a single feature vector, and this vector becomes an input for pattern recognition approaches such as neural networks, clustering or support vector machines. Finally, in decision-level fusion, decisions made by each sensor (or classifier) are fused for the final decision making. Feature-level fusion approaches are widely used for person identifications combining image features extracted from faces, hands and fingerprints (Chibelushi *et al.* 1997, Rose and Govindarajan 2005, Faundez-Zanuy 2005). Gunatilaka and Baertlein (2001) developed a land mine detection technique using feature-level and decision-level fusions. The reliability of linear ultrasonic based fatigue crack propagation monitoring is improved using feature-level fusion (Qiu *et al.* 2016). The features extracted using the baseline data obtained from the intact condition of the structure under various temperatures.

In this study, the reliability of ultrasonic modulation based fatigue crack detection is improved by fusing two features sensitive to fatigue crack: the spectral amplitude (SA) and the spectral correlation (SC). These features are extracted from ultrasonic responses obtained from a target structure when two ultrasonic inputs at distinct frequencies are applied. Then, a 2D feature space is constructed, and the damage classification is performed in the 2D feature space. The effectiveness of the proposed fatigue crack detection technique is experimentally validated using data obtained from aluminum plates, full-scale steel girders and a rotating shaft component. The reliability of the proposed technique is quantitatively investigated through receiver operating characteristic (ROC) analysis. Note that the proposed technique is suitable for field applications with harsh environmental conditions because it detects a fatigue crack without using baseline data obtained from intact condition of structure (reference-free). The uniqueness of this study lies in (1) improvement of nonlinear ultrasonic modulation based fatigue crack detection reliability using feature-level data fusion, (2) reference-free fatigue crack diagnosis without using the baseline data obtained from the intact condition of the structure, (3) application to full-scale steel girders and shaft component, and (4) quantitative investigation of the improved reliability using ROC

analysis.

This paper is organized as follows. Section 2 provides a brief introduction to the working principle of nonlinear ultrasonic modulation based fatigue crack detection. Section 3 describes the development of the reliability improved fatigue crack detection technique using feature-level data fusion. Then, experimental validations using the data obtained from aluminum plates, full-scale steel girders and a rotating shaft component are reported in Section 4. Quantitative investigation of the improved reliability of the developed fatigue crack detection technique and concluding remarks are provided in Sections 5 and 6, respectively.

2. Working principle of nonlinear ultrasonic modulation based fatigue crack detection

Consider two longitudinal plane waves a and b with distinct frequencies ω_a and ω_b ($\omega_a < \omega_b$) and amplitudes A_0 and B_0 . When they are applied to an intact (linear) structure in the z direction, the displacement of the waves, u_0 , can be written as

$$u_0 = A_0 \exp(i(\kappa_a z - \omega_a t)) + B_0 \exp(i(\kappa_b z - \omega_b t)) \quad (1)$$

where κ_a and κ_b are the wavenumbers of input waves a and b , respectively. The stress induced by the input waves (σ_0) becomes

$$\sigma_0 = E_0 \frac{\partial u_0}{\partial z} = E_0 [A_0^L \exp(i(\kappa_a z - \omega_a t)) + B_0^L \exp(i(\kappa_b z - \omega_b t))]i \quad (2)$$

where E_0 is the elastic modulus of the structure. A_0^L and B_0^L are the strain amplitudes induced by the input waves a and b , respectively.

An interaction between a localized fatigue crack and the applied input waves fluctuates the elastic modulus at the crack location (Donskoy *et al.* 2001). Thus, when a fatigue crack is located at z_0 , the elastic modulus fluctuation at z_0 , $E_1(z_0)$, can be expressed as (Lim and Sohn 2015)

$$E_1(z_0) = \bar{E}(z_0) + \alpha E_0 \frac{\partial u_0(z_0)}{\partial z} = \left[1 - \alpha \max\left(\frac{\partial u_0(z_0)}{\partial z}\right)\right] E_0 + \alpha E_0 \frac{\partial u_0(z_0)}{\partial z} \quad (3)$$

where $\bar{E}(z_0)$ is the average elastic modulus reduced from E_0 at z_0 , and α ($0 \leq \alpha < 1$) is the nonlinear coefficient representing the nonlinearity due to the fatigue crack. The max operation in Eq. (3) finds the maximum strain induced by the input waves at z_0 . Then, the stress at the crack location, σ_1 , can be derived as

$$\sigma_1 = E_1(z_0) \frac{\partial u_0(z_0)}{\partial z} = \left[1 - \alpha \max\left(\frac{\partial u_0(z_0)}{\partial z}\right)\right] E_0 \frac{\partial u_0(z_0)}{\partial z} + \alpha E_0 \left(\frac{\partial u_0(z_0)}{\partial z}\right)^2 \quad (4)$$

Substituting Eq. (1) into Eq. (4), the stress at the crack location due to the input waves becomes

$$\sigma_1 = \sigma_1^L + \sigma_1^H + \sigma_1^M \quad (5)$$

where σ_1^L , σ_1^H and σ_1^M are the stresses at ω_a and ω_b (linear), the nonlinear second harmonic components at $2\omega_a$ and $2\omega_b$ and the nonlinear modulation (first sideband) components at $\omega_a \pm \omega_b$, respectively. Each term can be written as

$$\sigma_1^L = E_0 [A_1^L \exp(i(\kappa_a z_0 - \omega_a t)) + B_1^L \exp(i(\kappa_b z_0 - \omega_b t))]i, \quad (6)$$

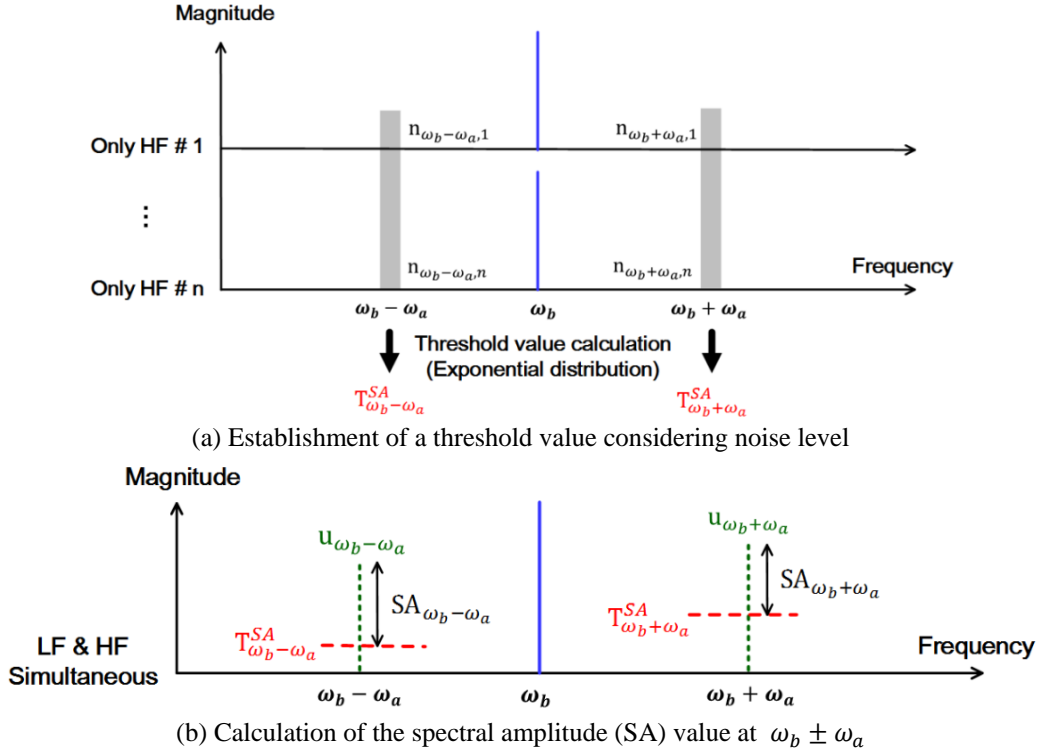


Fig. 1 Schematic diagram of the spectral amplitude (SA) value calculation

$$\sigma_1^H = -E_0[A_1^H \exp(2i(\kappa_a z_0 - \omega_a t)) + B_1^H \exp(2i(\kappa_b z_0 - \omega_b t))], \quad (7)$$

and

$$\sigma_1^M = -E_0 A_1^M \exp(i[(\kappa_b \pm \kappa_a) z_0 - (\omega_b \pm \omega_a) t]) \quad (8)$$

where A_1^L and B_1^L are the strain amplitudes of the linear responses, A_1^H and B_1^H are the strain amplitudes of the second harmonics, and A_1^M is the strain amplitudes of the modulation components. Using a more complex crack model considering additional square and cubic terms in Eq. (3), higher order harmonic and modulation components can be obtained. However, for simplicity, only the second harmonic and the first modulation terms are presented in this paper.

3. Improvement of crack detection reliability using feature-level data fusion

For field application of SHM techniques, damage diagnosis methods should be able to achieve high reliability by minimizing false alarms. Data fusion, i.e., combining data from multiple sensors (or information) to achieve improved accuracy compared to the use of a single sensor (or information) alone, is considered one way of improving fatigue crack diagnostic reliability. Thus, in this study, a fatigue crack detection method based on fusion of multiple features extracted from the data obtained from a single sensor (feature-level fusion), is developed for online SHM. First, two fatigue crack sensitive features, i.e., the spectral amplitude (SA) and the spectral correlation (SC), are

extracted from ultrasonic responses obtained from a target structure. Then, a 2D feature space is constructed, and the damage classification is performed in the feature space.

3.1 Feature extraction

Feature 1: Spectral Amplitude (SA)

The SA values are obtained by extracting the modulation amplitudes in the frequency domain. First, both LF and HF inputs are simultaneously applied to the structure, and the corresponding response at $\omega_b \pm \omega_a$ ($u_{\omega_b \pm \omega_a}$) are obtained. Next, as shown in Fig. 1(a), the additional ultrasonic response $n_{\omega_b \pm \omega_a}$ are obtained at $\omega_b \pm \omega_a$ by applying only the HF input considering the influence of the HF input on the noise level at $\omega_b \pm \omega_a$ (Lim *et al.* 2016). Here, $n_{\omega_b \pm \omega_a}$ are the sole outcome of the measurement noise because nonlinear modulation occurs only when HF and LF inputs are applied simultaneously. Then, the measurement of $n_{\omega_b \pm \omega_a}$ is repeated multiple times, and the n th noise value is denoted as $n_{\omega_b \pm \omega_a, n}$. Once multiple $n_{\omega_b \pm \omega_a, n}$ values are obtained, an exponential distribution is fitted to the $n_{\omega_b \pm \omega_a, n}$ values. Note that because the magnitude of the noise level is always positive in the frequency domain, an exponential distribution, which has only positive values, is selected here. After that, a threshold value, $T_{\omega_b \pm \omega_a}^{SA}$, corresponding to a user specified one-sided confidence interval is established as provided in Fig. 1(a).

Next, as presented in Fig. 1(b), the SA values at $\omega_b \pm \omega_a$ are defined

$$SA_{\omega_b \pm \omega_a} = u_{\omega_b \pm \omega_a} - T_{\omega_b \pm \omega_a}^{SA} \quad (9)$$

Finally, the SA value for the frequency combination of ω_a and ω_b is obtained by selecting the maximum value between $SA_{\omega_b - \omega_a}$ and $SA_{\omega_b + \omega_a}$:

$$SA_{\omega_b, \omega_a} = \max(SA_{\omega_b - \omega_a}, SA_{\omega_b + \omega_a}) \quad (10)$$

When the target structure is intact, $u_{\omega_b \pm \omega_a}$ will be smaller than $T_{\omega_b \pm \omega_a}^{SA}$, and the value of SA_{ω_b, ω_a} becomes negative. However, once a fatigue crack appears, $u_{\omega_b \pm \omega_a}$ will dramatically increase, and the value of SA_{ω_b, ω_a} will be positive. Thus, the SA value can be used as a feature for fatigue crack detection.

Feature 2: Spectral Correlation (SC)

In general, spectral correlation is used to identify the second-order (or wide-sense) cyclostationary stochastic processes whose autocorrelation functions vary periodically with time (Gardner 2006). To identify the crack-induced nonlinear modulations, the spectral correlation between two nonlinear modulation components at $\omega_b + \omega_a$ and $\omega_b - \omega_a$ (S_{ω_b, ω_a}) is obtained

$$S_{\omega_b, \omega_a} = E[X(\omega_b + \omega_a)X^*(\omega_b - \omega_a)] \quad (11)$$

where $X(\omega)$ is the Fourier transform of the structural response in the time domain. Note that the amplitudes of the modulation components are often at least ten to hundred times smaller than the amplitudes of the linear responses, and the nonlinear components are often varied under the noise level. Because the spectral correlation (SC) is less vulnerable to background random noise than is the conventional spectral density function in the frequency domain (Gardner 1986), the SC is selected as the second feature for extracting the nonlinear modulation components even under a high random noise level. The detailed signal processing procedure and description of the spectral correlation for nonlinear modulation are provided in Liu *et al.* (2016).

First, similar to the SA value calculation, S_{ω_b, ω_a} is obtained from the structural response when LF and HF inputs are simultaneously applied. Then, n spectral correlation values ($n_{\omega_b, \omega_a, n}$) are obtained by repeating the application of only the HF input. After that, a threshold value, $T_{\omega_b, \omega_a}^{SC}$, corresponding to a one-sided confidence interval is established by fitting an exponential distribution to $n_{\omega_b, \omega_a, n}$ values. Finally, the SC value for the input frequency combination of ω_a and ω_b is obtained

$$SC_{\omega_b, \omega_a} = S_{\omega_b, \omega_a} - T_{\omega_b, \omega_a}^{SC} \quad (12)$$

Similar to the SA value, the value of SC_{ω_b, ω_a} becomes negative when the target structure is intact. However, once a fatigue crack appears, S_{ω_b, ω_a} will dramatically increase and the value of SC_{ω_b, ω_a} will be positive. Thus, the SC value can also be used as a feature for fatigue crack detection.

3.2 Fatigue crack classification using feature-level fusion

By combining the SA and SC values extracted from the previous section, a damage classifier is developed using the following steps. The key advantage of the proposed damage classifier is that a fatigue crack is detected without using the baseline data obtained from the intact condition of the host structure.

STEP 1: Construction of a 2D feature space

First, as shown in Fig. 2(a), a 2D feature space is constructed using the SA and SC features normalized by their own standard deviations. When N combinations of two different input frequencies (data) are investigated, the i th data in the 2D feature space is expressed as

$$Z_i = (\overline{SA}_i, \overline{SC}_i) \quad i = 1, 2, \dots, N \quad (13)$$

where \overline{SA}_i and \overline{SC}_i are the i th normalized SA and SC features, respectively. Then, the data in the 1st quadrant are classified as the test data (Z^{test}), which indicates the generation of modulation components due to fatigue crack, and the remaining data in other quadrants are classified as the reference data (Z^{ref}). Note that, when Z_i falls into the 1st quadrant, both \overline{SA}_i and \overline{SC}_i values are positive, indicating a high chance of fatigue crack existence. When Z_i falls into the 3rd quadrant, most likely there is no fatigue crack. If the number of test data in the 1st quadrant is larger than the number of reference data in other quadrants, it implies much higher possibility of fatigue crack presence.

STEP 2: Novelty index calculation for the reference data

When the modulation components are generated at several frequency combinations due to fatigue crack, outlier analysis can be used for diagnosis of the fatigue crack (Lim *et al.* 2014). Before performing an outlier analysis on the test data with respect to the reference data, the closest distances among the reference data are measured using a Novelty Index (NI) (Fig. 2(b)). When the number of reference data is M , the NI value of the i th reference data (NI_i^{ref}) with respect to the other reference data can be written as

$$NI_i^{ref} = \min \left(\left\| Z_i^{ref} - Z_j^{ref} \right\|^2 \right) \quad i, j = 1, 2, \dots, M \quad (i \neq j) \quad (14)$$

Here, the min operation in Eq. (14) finds the closest distance from Z_i^{ref} with respect to the other reference data (Z_j^{ref}). Then, an exponential distribution is fitted to NI_i^{ref} values obtained from the reference data, and a threshold value corresponding to the one-sided confidence interval is estimated.

STEP 3: Novelty index calculation for the test data

Obtain the NI values of the test data with respect to the entire reference data as shown in Fig. 2(c). When the number of test data is K , the NI value for the k th test data (NI_k^{test}), defined as the closest distance from the k th test data (Z_k^{test}) to the entire reference data (Z^{ref}), can be expressed as

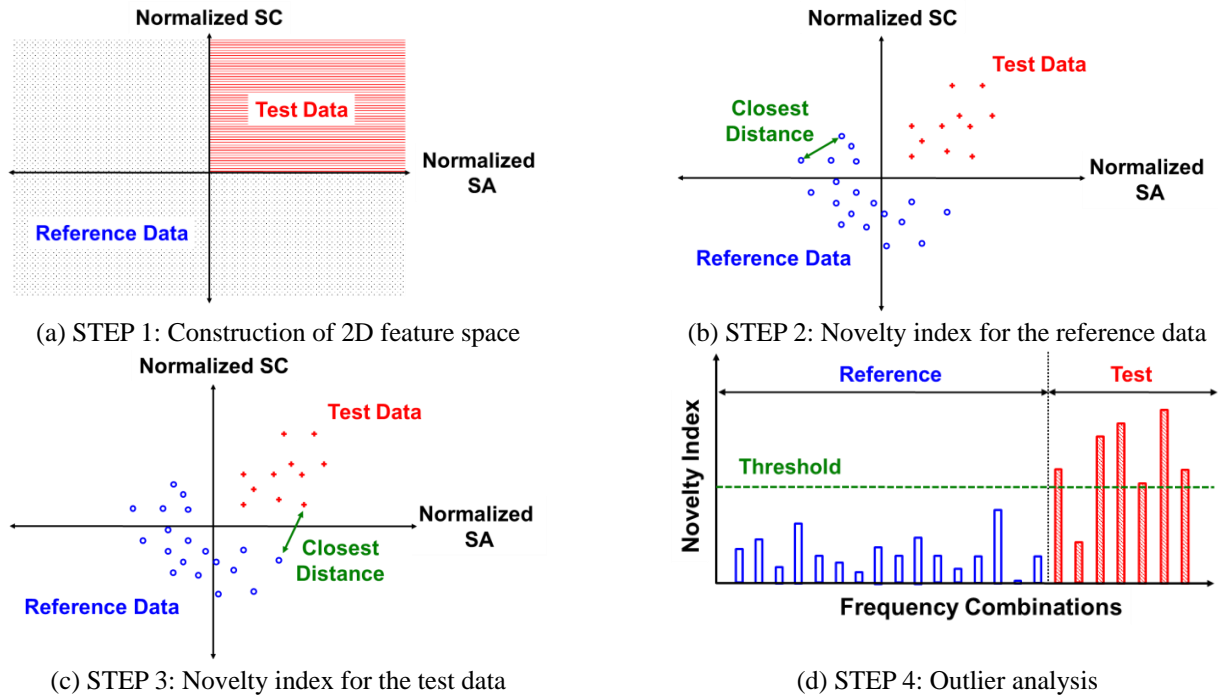


Fig. 2 Overview of the proposed outlier analysis based on the fusion of SA and SC features

$$NI_k^{test} = \min \left(\|Z_k^{test} - Z_j^{ref}\|^2 \right) \quad k = 1, 2, \dots, K \quad j = 1, 2, \dots, M \quad (15)$$

Similar to Eq. (14), the min operation in Eq. (15) finds the closest distance from Z_k^{test} with respect to the entire reference data.

STEP 4: Outlier analysis

Perform the outlier analysis using NI_k^{test} values for the test data and the threshold value obtained from STEP 2 (Fig. 2(d)). If any of NI_k^{test} values exceed the threshold value, it indicates the existence of a fatigue crack.

4. Experimental validation

4.1 Hardware configuration

In this study, a National Instrument (NI) PXI data acquisition (DAQ) system composed of two 16-bit arbitrary waveform generators (AWGs, NI PXI-5421) and a 14-bit, 2-channel high speed digitizer (DIG, NI PXI-5122) was used. AWGs were used to generate two zero-order holding sinusoidal LF and HF signals at ω_a and ω_b , respectively. The output responses were simultaneously measured using DIG at a sampling rate of 1 MHz. AWGs and DIG were synchronized and controlled by LabVIEW software. The responses were measured multiple times and averaged in the time domain to improve the signal-to-noise ratio.

4.2 Aluminum plate test

Two identical aluminum plate specimens with a notch were fabricated using 6061-T6 aluminum alloy as shown in

Fig. 3. The dimensions of the specimens were designed based on Korean Standard for fatigue test (KS B ISO 12108: 2004). Four identical PZTs manufactured by APC International were installed on each specimen. Each PZT has a diameter of 25 mm and a thickness of 0.5 mm. Two PZTs labeled LF and HF were used for the generation of ultrasonic inputs at ω_a and ω_b , respectively, and the other two, denoted SEN 1 and SEN 2, were used for sensing. The specimens were subjected to cyclic loading tests using an MTS machine with a 10 Hz cycle rate and a load of 3.5~35 kN (stress ratio $R=0.1$).

Both LF and HF input signals had a 0.1 sec duration and a peak-to-peak voltage of ± 2 V. For aluminum plate I, various input frequency combinations were investigated by sweeping ω_a from 40 to 50 kHz and ω_b from 193 to 195 kHz both with 1 kHz increment, respectively. The sweeping ranges of the input signals were determined by considering the local resonance characteristics of the specimen. The output responses with a duration of 0.1 sec were obtained 10 times and averaged.

Fig. 4 shows the frequency domain responses of the raw signals obtained from SEN 2 of aluminum plate I. This figure shows that the intrinsic material nonlinearity is negligible for the tested aluminum specimen (0k cycles, 0.00 mm crack length), and the modulation components become apparent when a fatigue crack with a length of 31.64 mm is formed after applying 44k cycles of fatigue loading. Fig. 5 shows the modulation amplitudes obtained from SEN 2 of aluminum plate I when ω_a was swept from 40 to 50 kHz and ω_b was swept from 193 to 195 kHz. Similar to Fig. 4, a higher level of modulation was observed at certain frequency combinations when the fatigue crack was formed after applying 44k cycles of fatigue loading (31.64 mm crack length).

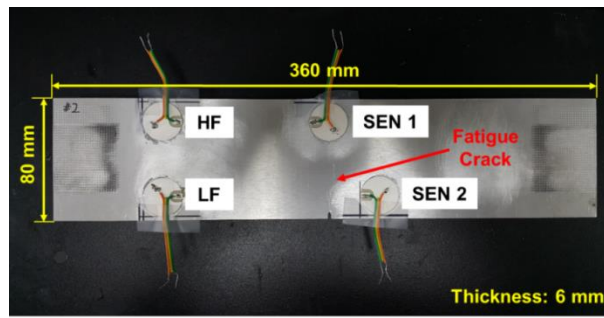
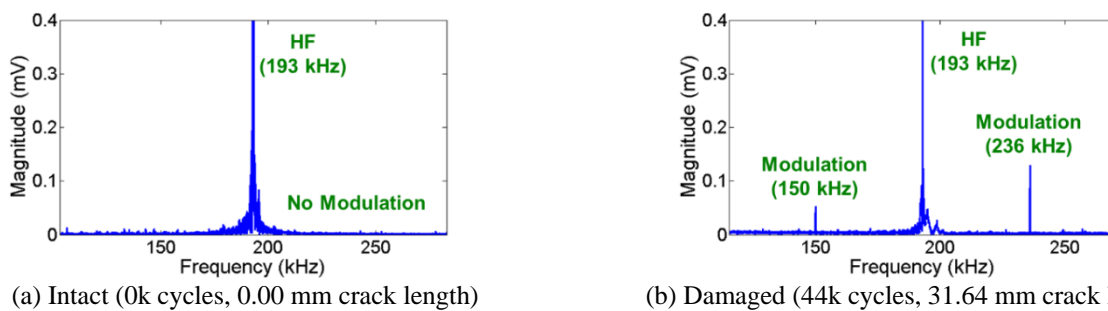


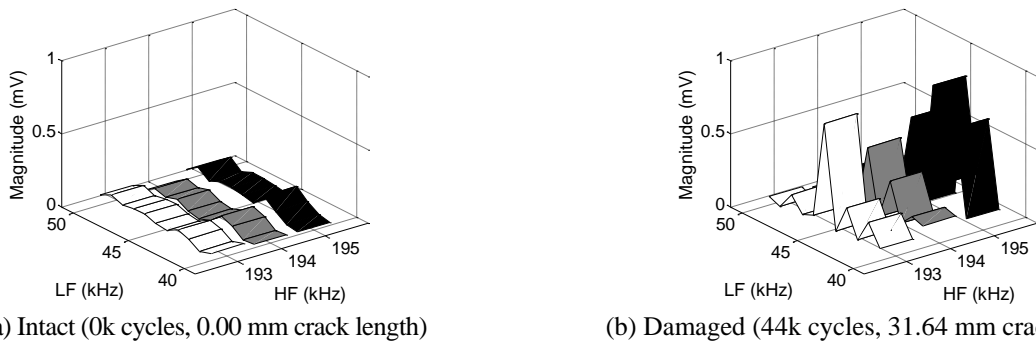
Fig. 3 Dimension of the aluminum plate specimen and PZT installation. Two PZTs labeled LF and HF were used for the generation of ultrasonic inputs at ω_a and ω_b , respectively, and the other two denoted as SEN 1 and SEN 2 were used for sensing



(a) Intact (0k cycles, 0.00 mm crack length)

(b) Damaged (44k cycles, 31.64 mm crack length)

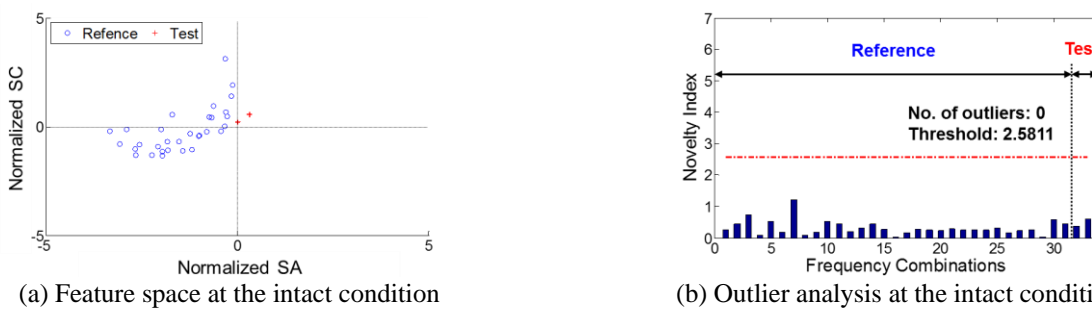
Fig. 4 Modulation amplitude in the frequency domain when $\omega_a = 43$ kHz and $\omega_b = 193$ kHz are applied simultaneously (from SEN 2 of aluminum plate I)



(a) Intact (0k cycles, 0.00 mm crack length)

(b) Damaged (44k cycles, 31.64 mm crack length)

Fig. 5 Modulation amplitudes within the investigated frequency bands when ω_a was swept from 40 to 50 kHz and ω_b from 193 to 195 kHz (from SEN 2 of aluminum plate I)



(a) Feature space at the intact condition

(b) Outlier analysis at the intact condition

Fig. 6 Visualization of the SA and SC features in the 2D feature space and the outlier analysis performed on the data obtained from SEN 2 of the intact condition of aluminum plate I (0k cycles, 0.00 mm crack length)

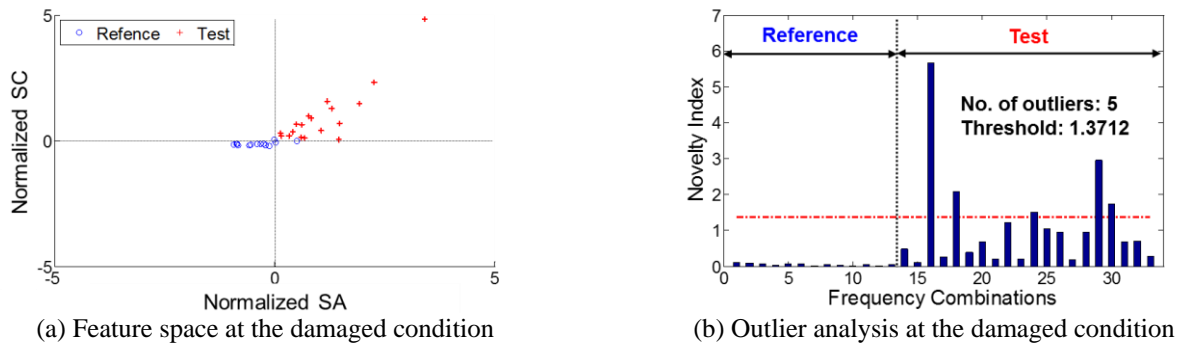


Fig. 7 Visualization of the SA and SC features in the 2D feature space and the outlier analysis performed on the data obtained from SEN 2 of the damaged condition of aluminum plate I (38k cycles, 11.63 mm crack length)

Table 1 Damage detection results for aluminum plate I

Cycles	SM Analysis	SC Analysis	Fusion (No. of outliers)	Real condition (Crack length)
0k	SEN 1	Intact	Intact (0)	Intact (0.00 mm)
	SEN 2	Intact	Intact (0)	
5k	SEN 1	Damage	Damage (1)	Damage (0.50 mm)
	SEN 2	Damage	Damage (5)	
10k	SEN 1	Damage	Damage (4)	Damage (1.00 mm)
	SEN 2	Damage	Damage (5)	
18k	SEN 1	Damage	Damage (4)	Damage (1.31 mm)
	SEN 2	Damage	Damage (5)	
23k	SEN 1	Damage	Damage (4)	Damage (2.54 mm)
	SEN 2	Damage	Damage (4)	
28k	SEN 1	Damage	Damage (1)	Damage (4.29 mm)
	SEN 2	Damage	Damage (5)	
33k	SEN 1	Damage	Damage (4)	Damage (6.84 mm)
	SEN 2	Damage	Damage (2)	
38k	SEN 1	Damage	Damage (2)	Damage (11.63 mm)
	SEN 2	Damage	Damage (5)	
42k	SEN 1	Damage	Damage (1)	Damage (19.26 mm)
	SEN 2	Damage	Damage (2)	
43k	SEN 1	Damage	Damage (6)	Damage (22.95 mm)
	SEN 2	Damage	Damage (4)	
44k	SEN 1	Damage	Damage (4)	Damage (31.64 mm)
	SEN 2	Damage	Damage (6)	

Fig. 6(a) visualizes the SA and SC features obtained from SEN 2 of aluminum plate I in the 2D feature space when there was no fatigue crack (0k, 0.00 mm crack length). A 99.999% confidence interval was used throughout the test to obtain the SA, SC and threshold values. Fig. 6(b) shows the results of the outlier analysis performed on the data in Fig. 6(a). Only 2 data were located in the 1st quadrant, and no outlier was observed. After applying 38k cycles of loading, a 11.63 mm long crack was formed. At this crack length, over 50% of the data (20 out of 33) were located in the 1st quadrant (Fig. 7(a)), and 5 outliers were observed, as shown in Fig. 7 (b).

The data were obtained periodically during the fatigue test, and the presence of fatigue cracks was confirmed by

visual inspection. A fatigue crack was initiated after applying 4k cycles of loading, and the crack length measurement at each DAQ was performed using a digital Vernier calipers. The measured crack length and the damage detection results are presented in Table 1. The performance of the developed feature-level fusion based classifier is compared with the Skewness-Median (SM) analysis developed by Lim *et al.* (2016) and the Spectral Correlation (SC) analysis develop by Liu *et al.* (2016). Note that the SM analysis is a classifier solely based on the SA value, and the SC analysis is based only on the SC value. The results indicate that reliable fatigue crack detection results are achieved when feature-level fusion is applied.

Table 2 Damage detection results for aluminum plate II

Cycles		SM Analysis	SC Analysis	Fusion (No. of outliers)	Real condition (Crack length)
0k	SEN 1	Intact	Intact	Intact (0)	Intact (0.00 mm)
	SEN 2	Intact	Intact	Intact (0)	
3k	SEN 1	Damage	Damage	Damage (2)	Damage (0.32 mm)
	SEN 2	Damage	Damage	Damage (3)	
6k	SEN 1	Damage	Damage	Damage (3)	Damage (0.69 mm)
	SEN 2	Damage	Damage	Damage (6)	
9k	SEN 1	Damage	Damage	Damage (3)	Damage (1.73 mm)
	SEN 2	Damage	Damage	Damage (4)	
12k	SEN 1	Damage	Damage	Damage (1)	Damage (2.99 mm)
	SEN 2	Damage	Damage	Damage (2)	
15k	SEN 1	Damage	Damage	Damage (1)	Damage (4.51 mm)
	SEN 2	Damage	Damage	Damage (6)	
18k	SEN 1	Damage	Damage	Damage (3)	Damage (5.68 mm)
	SEN 2	Damage	Damage	Damage (4)	
21k	SEN 1	Damage	Damage	Damage (2)	Damage (6.89 mm)
	SEN 2	Damage	Damage	Damage (3)	
24k	SEN 1	Damage	Damage	Damage (1)	Damage (10.10 mm)
	SEN 2	Damage	Damage	Damage (3)	

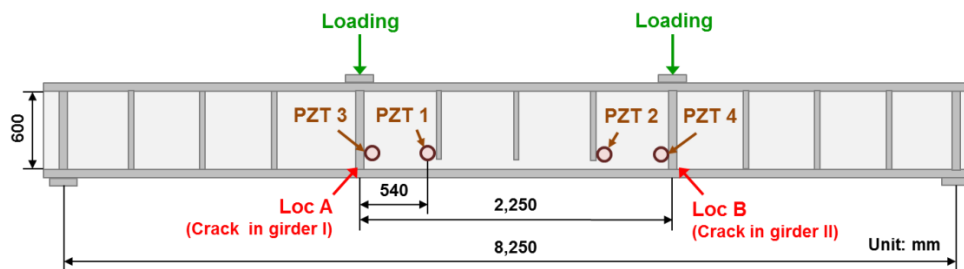


Fig. 8 Dimensions of the full-scale steel girder and PZT installation

For aluminum plate II, ω_a was stepped from 30 to 40 kHz and ω_b from 187 to 189 kHz both with 1 kHz increment. The other DAQ parameters were identical to those of aluminum plate I. The measured crack length and the fatigue crack diagnosis results obtained from aluminum plate II are presented in Table 2. Similar to aluminum plate I, reliable damage diagnosis results are obtained when the features are combined. The experimental results of the aluminum plates show that the proposed technique detects small fatigue crack less than 0.5 mm length.

4.3 Full-scale steel girder test

Two identical steel girders were fabricated, and the dimensions are presented in Fig. 8. For the steel girder tests, triple PZT modules designed by the authors and manufactured by Metis Design were used. The triple PZT module consists of three identical circular PZTs packaged by Kapton tape with a printed circuit and three SMA connectors. A detailed description of the triple PZT module is presented in Lim *et al.* (2016). Potential crack initiation locations were predicted by finite element analysis in the design stage of the girders, and two triple PZT modules (PZTs 1 and 2) were installed near the expected crack

locations for each girder before applying fatigue loading, as shown in Fig. 8.

For girder I, the fatigue test was performed using an MTS machine with a 1 Hz cycle rate and a cyclic load of 287~712 kN. After every 100k cycles, a static load of 712 kN was applied to examine the formation of fatigue crack.

The presence of an invisible closed crack can be visually inspected by opening the crack applying a constant static loading. Both LF and HF input signals had a peak-to-peak voltage of ± 12 V. The other DAQ parameters were identical to those of the aluminum plates. For each PZT, the frequency response function at each PZT installation location was measured and the sweeping frequency range was selected to capture as many local resonance frequencies as possible. In this way, ω_a was stepped from 30 to 40 kHz and ω_b from 182 to 184 kHz, both with 1 kHz increment for PZT 1. For PZT 2, ω_a was stepped from 40 to 50 kHz, and ω_b was stepped from 181 to 183 kHz both with 1 kHz increment.

As shown in Fig. 9, the displacement curve obtained from the MTS machine during the fatigue test shows the typical fatigue crack growth behavior of metals in fracture mechanics (Anderson 2005). It is estimated that an invisible fatigue crack initiated around 400k cycles. From 400k

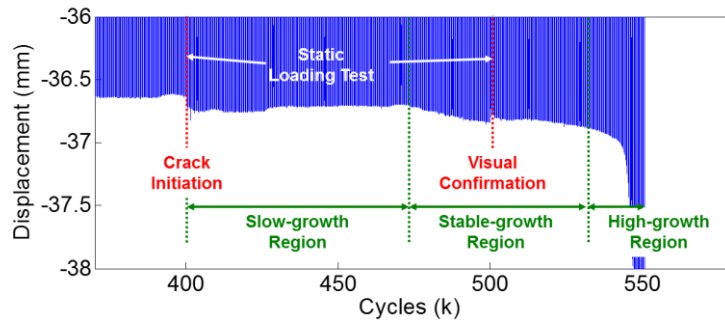


Fig. 9 A fatigue cycle vs. displacement curve obtained from the MTS machine during the fatigue test of girder I (zoomed in for the displacement range of -36 mm to -38 mm)

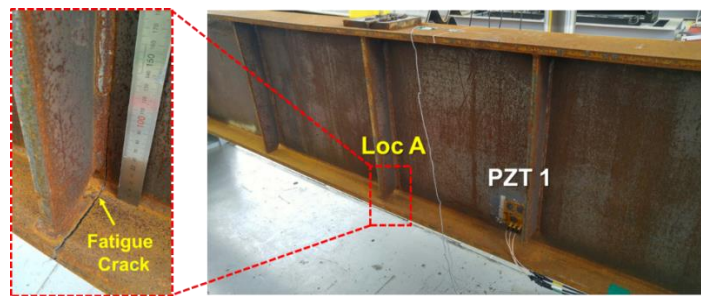


Fig. 10 Visual confirmation of a fatigue crack after 550k cycles of loading (Loc A of girder I)

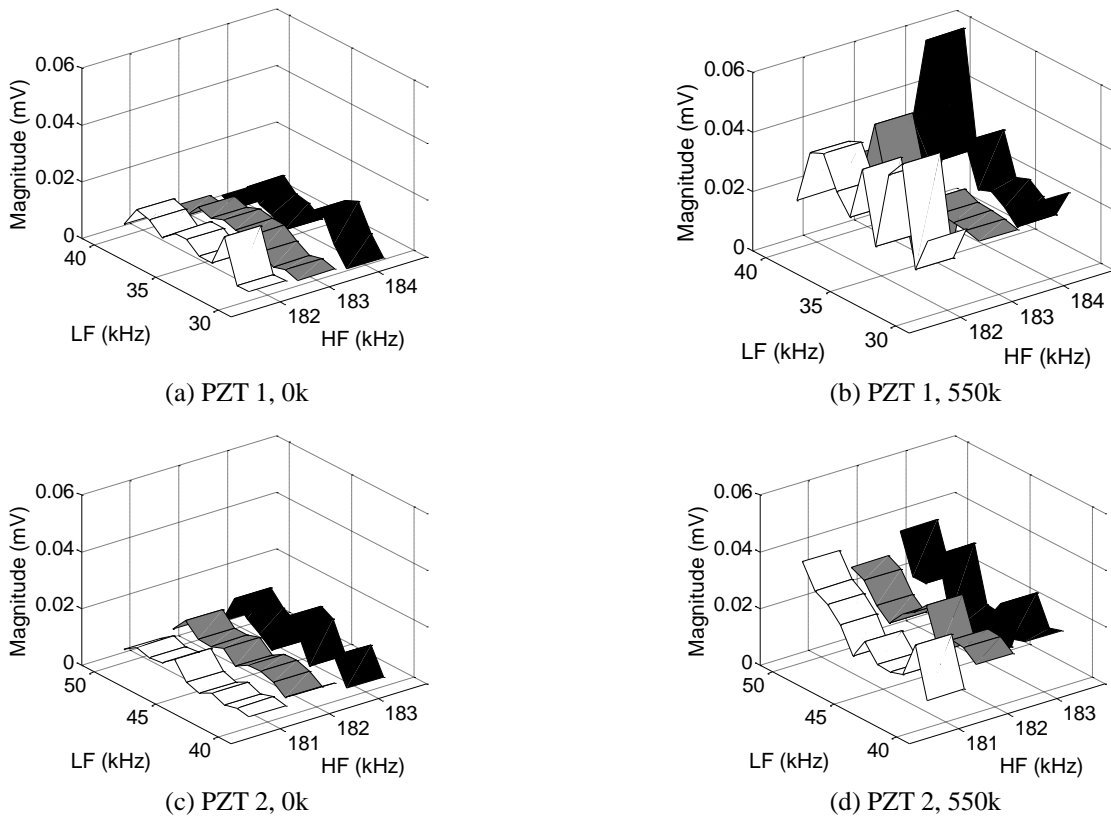


Fig. 11 Modulation amplitudes obtained from girder I. For PZT 1, ω_a was swept from 30 to 40 kHz and ω_b from 182 to 184 kHz. ω_a was swept from 40 to 50 kHz, and ω_b from 181 to 183 kHz for PZT 2. The sweeping ranges of the input frequencies were determined by considering the local resonance characteristics of each PZT installation location

Table 3 Damage detection results for girder I

Cycles		SM Analysis	SC Analysis	Fusion (No. of outliers)	Real Condition
0k	PZT 1	Intact	Damage	Intact (0)	Intact
	PZT 2	Damage	Damage	Intact (0)	
300k	PZT 1	Intact	Intact	Intact (0)	Intact
	PZT 2	Intact	Intact	Intact (0)	
400k	PZT 1	Damage	Damage	Damage (2)	Damage (Loc A)
	PZT 2	Intact	Damage	Intact (0)	
500k	PZT 1	Damage	Damage	Damage (2)	Damage (Loc A)
	PZT 2	Damage	Damage	Damage (5)	
550k	PZT 1	Damage	Damage	Damage (1)	Damage (Loc A)
	PZT 2	Damage	Damage	Damage (1)	

Table 4 Additional damage detection results for girder I after 550k cycles

Path (Excitation – Sensing)	SM Analysis	SC Analysis	Fusion (No. of outliers)
PZT 1 – PZT 3	Damage	Damage	Damage (1)
PZT 1 – PZT 4	Damage	Damage	Damage (1)
PZT 2 – PZT 3	Damage	Damage	Damage (2)
PZT 2 – PZT 4	Damage	Damage	Damage (1)

Table 5 Damage detection results for girder II

Cycles		SM Analysis	SC Analysis	Fusion (No. of outliers)	Real Condition
0k	PZT 1	Intact	Damage	Intact (0)	Intact
	PZT 2	Intact	Damage	Intact (0)	
20k	PZT 1	Intact	Damage	Intact (0)	Damage (Loc B)
	PZT 2	Damage	Damage	Damage (1)	
40k	PZT 1	Damage	Damage	Damage (15)	Damage (Loc B)
	PZT 2	Damage	Damage	Damage (3)	

cycles, the crack slowly grew until 470k cycles (slow-growth region, Region I). After 470k cycles, the fatigue crack began to propagate in earnest (stable-growth region, Region II). Around 500k cycles, the existence of the fatigue crack was visually confirmed at Loc A (Fig. 10). Around 550k cycles, the crack grew rapidly (high-growth region, Region III).

Fig. 11 presents the modulation amplitudes at multiple frequency combinations obtained from PZTs 1 and 2 under the intact (0k cycles) and damaged (after 550k cycles) conditions, respectively. Similar to the aluminum plates, the modulation components are generated by the presence of the fatigue crack. Additionally, a higher modulation level was obtained at PZT 1.

Ultrasonic responses were acquired periodically during the fatigue test, and the damage detection results are presented in Table 3. A 99.999% confidence interval was applied throughout the test to obtain the SA, SC and threshold values. Similar to the aluminum plates, more reliable fatigue crack detection results are obtained when the proposed technique is applied.

To confirm the formation of the fatigue crack, two additional PZTs labelled as PZTs 3 and 4 were placed near Locs A and B after 550k cycles as shown in Fig. 8. Pitch-catch signals were obtained from PZTs 3 and 4 by exciting PZTs 1 and 2, respectively. Here, the excitation frequency ranges of PZTs 1 and 2 were identical to the previous damage detection tests. Fig. 12 shows that higher modulation amplitudes were observed from PZT 1 – PZT 3 pitch-catch signal rather than PZT 2 – PZT 4 pitch-catch signal. Based on the observation, it is speculated that the fatigue crack is formed at Loc A rather than Loc B or at least the crack at Loc A is larger than the one at Loc B. Additional pitch-catch signals were obtained by exciting PZT 2 and measuring the response at PZT 3 to confirm that ultrasonic response can propagate for about 1.7 m distance between PZT 2 and PZT 3 and detect the fatigue crack. The identical result is also obtained from the pitch-catch signal from PZT 1 to PZT 4. It is concluded that the modulation observed at PZT 2 is also caused by the fatigue crack at Loc A. The additional damage diagnosis results are shown in Table 4.

Table 6 Damage detection results for girder II after 40k cycles

Path (Excitation – Sensing)	SM Analysis	SC Analysis	Fusion (No. of outliers)
PZT 1 – PZT 3	Damage	Damage	Damage (12)
PZT 1 – PZT 4	Damage	Damage	Damage (3)
PZT 2 – PZT 3	Damage	Damage	Damage (1)
PZT 2 – PZT 4	Damage	Intact	Damage (4)

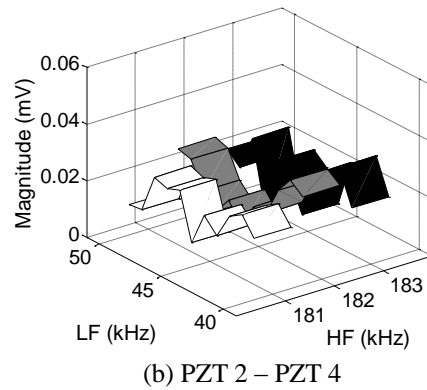
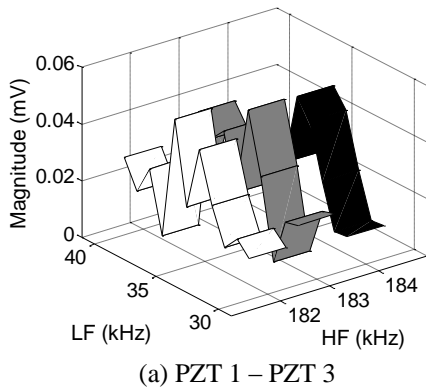
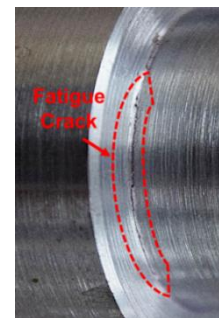
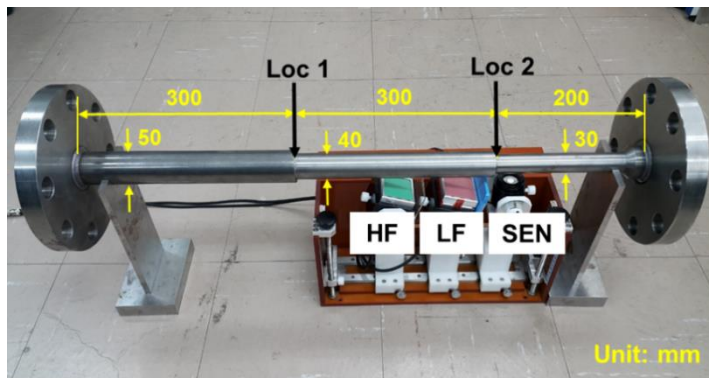


Fig. 12 Modulation amplitudes obtained from pitch-catch signals on girder I. (a) between PZT 1 (excitation) and PZT 3 (sensing) and (b) between PZT 2 (excitation) and PZT 4 (sensing)



(a) Dimensions of the aluminum shaft specimen and ACT installation

(b) Fatigue crack at Loc 2

Fig. 13 Aluminum shaft specimen test

Table 7 Damage detection results for the aluminum shaft specimen

Cycles	SM Analysis	SC Analysis	Fusion (No. of outliers)	Real Condition	
0.0k	Loc 1	Damage	Intact	Intact (0)	Intact
	Loc 2	Damage	Intact	Intact (0)	
1.5k	Loc 1	Damage	Intact	Intact (0)	Intact
	Loc 2	Damage	Intact	Intact (0)	
3.0k	Loc 1	Damage	Intact	Intact (0)	Intact
	Loc 2	Damage	Intact	Intact (0)	
4.5k	Loc 1	Damage	Intact	Intact (0)	Intact
	Loc 2	Damage	Intact	Intact (0)	
6.0k	Loc 1	Damage	Intact	Intact (0)	Damage (Loc 2)
	Loc 2	Damage	Intact	Damage (1)	

For girder II, a 139~860 kN cyclic loading with a 1 Hz cycle rate was applied. For an independent confirmation of fatigue crack formation, a static load of 860 kN was applied every 20k cycles. For PZT 1, ω_a was stepped from 40 to 50 kHz and ω_b from 189 to 191 kHz, both with 1 kHz increment. For PZT 2, ω_a was stepped from 40 to 50 kHz and ω_b from 181 to 183 kHz. The other DAQ parameters were identical to those for girder I.

Based on the displacement measured by the MTS machine during the fatigue test, it is estimated that a fatigue crack initiated around 10k cycles. After 40k cycles, the fatigue crack was visually observed at Loc B. Thus, the additional test was also conducted in the same manner. As shown in Tables 5 and 6, the fatigue crack is successfully detected using the proposed technique similar to the results for girder I, and it is validated that the modulation component is generated due to the presence of the fatigue crack at Loc B.

4.4 Aluminum shaft test

The proposed technique was also examined a rotating shaft specimen that is widely used for drop-lifts in car manufacturing factories (Fig. 13(a)). The 1/4 scale shaft specimen was fabricated using 6061-T6 aluminum alloy and a cyclic torsional loading of 0~3 kN·m with a 1 Hz cycle rate was applied. The data were obtained periodically during the fatigue test, and the presence of fatigue cracks was monitored periodically examined by the visual inspection and the angular displacement recorded by the MTS machine. After 6,000 cycles, a fatigue crack was introduced at Loc 2 as shown in Fig. 13(b).

For applying LF and HF inputs to the shaft specimen, non-contact air-coupled transducers (ACTs) NCG50-S38 and NCG200-S38 manufactured by the Ultrason Group were used. A BAT-1 ACT (MicroAcoustics Co.) was used to obtain the corresponding responses. Note that the ACTs were used in this experiment because the real target shaft will be in rotation conditions most of times. The ACTs were approximately 50 mm away from the shaft surface, and their incidence angles were set to be approximately 3° from the vertical direction. For Loc 1, ω_a was stepped from 50 to 60 kHz and ω_b from 201 to 203 kHz, both with 1 kHz increment. For Loc 2, ω_a was stepped from 40 to 50 kHz and ω_b from 197 to 199 kHz. Both the LF and HF input signals had a 0.5 sec duration and a peak-to-peak voltage of ± 50 V. The 0.5 sec duration output responses were obtained 15 times and averaged. A 90% confidence interval was applied to obtain the SA, SC and threshold values. Note that, because of the higher level of noise and lower level of modulation obtained by the ACTs compared to the previous PZTs, the confidence level was adjusted in this example. Table 7 shows the fatigue crack detection results for the aluminum shaft specimen. Similar to the previous tests, reliable fatigue crack detection results are obtained.

5. Fatigue crack detection reliability analysis

The fatigue crack detection reliability of the proposed

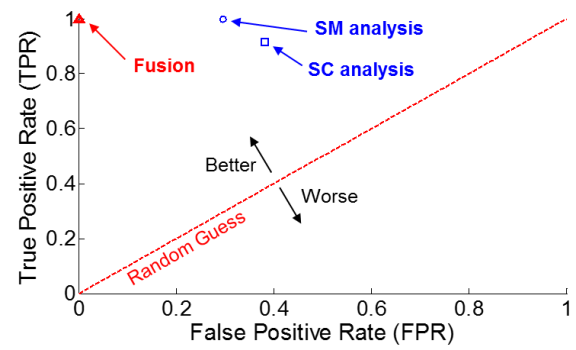


Fig. 14 The receiver operating characteristic (ROC) space for the damage detection reliability analysis

fatigue crack detection technique was analyzed by comparing the reliability of the SM analysis and the SC analysis. An ROC space, which illustrates the performance of a binary classifier, is created using all of the fatigue crack diagnosis results presented in this study. The ROC space is defined by the false positive rate (FPR) and the true positive rate (TPR) as the x and y axes, respectively, and it depicts the relative trade-offs between true positive (TP) and false positive (FP) (Fawcett 2006). In this study, TP denotes correctly classifying a structure with a fatigue crack as damaged, while FP denotes falsely classifying for an intact structure as damaged. In the ROC space, the classifier with perfect classification would be located at the coordinate of (0,1) (the upper left corner). A completely random guess (e.g., flipping coins) would give a point along a diagonal line from the left bottom to the top right corners. Fig. 14 presents the ROC space for the damage detection reliability analysis. Here, damage classification is defined successful if damage is detected by at least one of the PZTs installed on target structure. For example, the crack was successfully detected by PZT 2 at 400k cycles for girder I shown in Table 3 (PZT 1 at 20k cycles for girder II provided in Table 5 and Loc 1 at 6k cycles for the shaft in Table 7). This classification seems to be reasonable because we cannot expect that damage be always detected by both PZTs. Note that, in the full-scale steel girder, the crack was formed near PZT 1 and PZT 2 is 1.6 m apart from the crack. The proposed feature-level fusion based fatigue crack detection technique shows better classification than the SM and SC analyses for the presented tests. The SC analysis shows a more conservative damage detection performance (higher false positive rate) than the SM analysis.

6. Conclusions

In this study, the reliability of nonlinear ultrasonic modulation based fatigue crack detection is improved using a feature-level data fusion. As damage sensitive features, the spectral amplitude and the spectral correlation values are extracted from the ultrasonic response obtained when two ultrasonic inputs at distinct frequencies are applied simultaneously. Then, a 2D feature space is constructed, and damage classification is performed in the 2D feature space

using an outlier analysis. The effectiveness of the proposed fatigue crack detection technique is experimentally validated using the data obtained from aluminum plates, full-scale steel girders and a rotating shaft specimen. Then, the improved reliability of the proposed technique is quantitatively investigated through receiver operating characteristic analysis. The uniqueness of this study lies in (1) improvement of nonlinear ultrasonic modulation based fatigue crack detection reliability using feature-level data fusion, (2) reference-free fatigue crack diagnosis without using the baseline data obtained from the intact condition of the structure, (3) application to full-scale steel girders and shaft component, and (4) quantitative investigation of the improved reliability using receiver operating characteristic analysis.

Acknowledgments

This research was supported by the Field-oriented Support of Fire Fighting Technology Research and Development Program funded by the Ministry of Public Safety and Security (MPSS- firesafety--2015-72).

References

- Amerini, F. and Meo, M. (2011), "Structural health monitoring of bolted joints using linear and nonlinear acoustic/ultrasound methods", *Struct. Health Monit.*, **10**(6), 659-672.
- Anderson, T. L. (2005), *Fracture Mechanics – Fundamentals and Applications*, 3rd edition, CRC Press, Boca Raton, FL, USA.
- Cammarata, M., Rizzo, P., Dutta, D. and Sohn, H. (2010), "Application of principal component analysis and wavelet transform to fatigue crack detection in waveguides", *Smart Struct. Syst.*, **6**(4), 349-362.
- Campbell, F.C. (2008), *Elements of Metallurgy and Engineering Alloys*, ASM International, Materials Park, OH, USA.
- Cantrell, J.H. and Yost, W.T. (1994), "Acoustic harmonics generation from fatigue-induced dislocation dipoles", *Philos. Mag. A*, **69**(2), 315-326.
- Chibelushi, C.C., Mason, J. S. D., Deravi F. (1997), "Feature-level data fusion for bimodal person recognition", *Proceedings of the 6th International Conference on Image Processing and Its Applications*, Dublin, July.
- Chrysochoidis, N.A., Barouni, A.K. and Saravanos, D.A. (2011), "Delamination detection in composites using wave modulation spectroscopy with a novel active nonlinear acousto-ultrasonic piezoelectric sensor", *J. Intel. Mat. Syst. Str.*, **22**(18), 2193-2206.
- Croxford, A.J., Wilcox, P.D., Drinkwater, B.W., Nagy, P.B. (2009), "The use of non-collinear mixing for nonlinear ultrasonic detection of plasticity and fatigue", *J. Acoust. Soc. Am. EL*, **126**(5), 117-122.
- Donskoy, D., Sutin, A. and Ekimov, A. (2001), "Nonlinear acoustic interaction on contact interfaces and its use for nondestructive testing", *NDT E. Int.*, **34**(4), 231-238.
- Duffour, P., Morbidini, M. and Cawley, P. (2006), "A study of the vibro-acoustic modulation technique for the detection of cracks in metals", *J. Acoust. Soc. Am.*, **119**(3), 1463-1475.
- Faundez-Zanuy, M. (2005), "Data fusion in biometrics", *IEEE Aero. El. Sys. Mag.*, **20**(1) 34-38.
- Fawcett, T. (2006), "An introduction to ROC analysis", *Pattern Recognit. Lett.*, **27**, 861-874.
- Gardner, W.A. (1986), "Measurement of spectral correlation", *IEEE T. Acoust. Speech Signal Process.*, **34**, 1111-1123.
- Gardner, W.A. (2006), "Cyclostationarity: Half a century of research", *Signal Process.*, **86**, 639-697.
- Gunatilaka, A.H. and Baertlein B.A. (2001), "Feature-level and decision-level fusion of noncoincidentally sampled sensors for land mine detection", *IEEE T. Pattern Anal.*, **23**(6), 577-589.
- Hall, D.L. and Llinas, J. (1997), "An introduction to multi-sensor data fusion", *Proceedings of the IEEE*, **85**(1), 6-23.
- Hong, M., Wang, Q., Su, Z., Cheng, L. (2014), "In situ health monitoring for bogie systems of CRH380 train on Beijing-Shanghai high-speed railway", *Mech. Syst. Signal Process.*, **45**, 378-395.
- Jhang, K.Y. (2009), "Nonlinear ultrasonic techniques for nondestructive assessment of micro damage in material: A review", *Int. J. Precis. Eng. Manuf.*, **10**(1), 123-135.
- JST Failure Knowledge Database (2016), Collapse of the Korea Seoul Seongsu Bridge; Hatamura Institute for the Advancement of Technology, Japan. <http://www.sozogaku.com/fkd/en/>
- Kim, J.M., Han, M., Lim, H.J., Yang, S. and Sohn, H. (2016), "Operation of battery-less and wireless sensor using magnetic resonance based wireless power transfer through concrete", *Smart Struct. Syst.*, **17**(4), 631-646.
- Kim, J. Y., Jacobs, L. J., Qu, J. (2011), "Nonlinear ultrasonic techniques for nondestructive damage assessment in metallic materials", *Proceedings of the 8th International Workshop on Structural Health Monitoring*, Stanford, CA, September.
- Klepka, A., Staszewski, W.J., Jenal, R.B., Szewdo, M., Iwaniec, J. (2011), "Nonlinear acoustics for fatigue crack detection – experimental investigations of vibro-acoustic wave modulations", *Struct. Health Monit.*, **11**(2), 197-211.
- KS B ISO 12108 (2004), *Metallic materials – Fatigue testing – Fatigue crack growth method*, Korean Agency for Technology and Standard (KATS); Seoul, South Korea.
- Lim, H.J. and Sohn, H. (2015), "Fatigue crack detection using structural nonlinearity reflected on linear ultrasonic features", *J. Appl. Phys.*, **118**, 244902.
- Lim, H.J., Kim, Y., Koo, G., Yang, S., Sohn, H., Bae, I.H. and Jang, J.H. (2016), "Development and field application of a nonlinear ultrasonic modulation technique for fatigue crack detection without reference data from an intact condition", *Smart Mater. Struct.*, **25**, 095055.
- Lim, H.J., Sohn, H., DeSimio, M.P. and Brown, K. (2014), "Reference-free fatigue crack detection using nonlinear ultrasonic modulation under various temperature and loading conditions", *Mech. Syst. Signal Process.*, **45**(2), 468-478.
- Liu, P., Sohn, H., Yang, S. and Lim, H.J. (2016), "Baseline-free fatigue crack detection based on spectral correlation and nonlinear wave modulation", *Smart Mater. Struct.*, Accepted.
- Parsons, Z. and Staszewski, W.J. (2006), "Nonlinear acoustics with low-profile piezoceramic excitation for crack detection in metallic structures", *Smart Mater. Struct.*, **15**, 1110-1118.
- Qiu, L., Yuan, S., Bao, Q., Mei, H. and Ren, Y. (2016), "Crack propagation monitoring in a full-scale aircraft fatigue test based on guided wave-Gaussian mixture model", *Smart Mater. Struct.*, **25**(5), 055048.
- Rose, A.A. and Govindarajan, R. (2005), "Feature level fusion of hand and face biometrics", *Proceedings of SPIE Biometric Technology for Human Identification II*, Orlando, April.
- Sohn, H., Lim, H.J., DeSimio, M.P., Brown, K. and Derriso, M. (2014), "Nonlinear ultrasonic wave modulation for online fatigue crack detection", *J. Sound Vib.*, **333**(5), 1473-1484.
- Yim, H.J., Park, S.J., Kim, J.H. and Kwak, H.G. (2016), "Evaluation of freezing and thawing damage of concrete using a nonlinear ultrasonic method", *Smart Struct. Syst.*, **17**(1), 45-58.
- Yoder, N.C. and Adams, D.E. (2010), "Vibro-acoustic modulation

using a swept probing signal for robust crack detection”, *Struct. Health Monit.*, **9**(3), 257-267.

Zhou, C., Hong, M., Su, Z., Wang, Q. and Cheng, L. (2013), “Evaluation of fatigue cracks using nonlinearities of acousto-ultrasonic waves acquired by an active sensor network”, *Smart Mater. Struct.*, **22**, 015018.

HJ